Minimizing the RF Fields on the Surface of an SRF Cavity by Optimizing its Shape

David Stark[1,2], Valery Shemelin[2]

[1]*School of Physics and Astronomy, University of Minnesota, Minneapolis, MN, 55455,*

[2]*Cornell Laboratory for Accelerator-Based Sciences and Education,*

Cornell University, Ithaca, NY 14853

Accelerating gradients in SRF cavities have consistently been increasing in recent years, largely due to better surface preparation techniques. This makes the critical magnetic field, at which the cavity loses its superconductivity, a very important limit to address. We worked to minimize the peak magnetic field H_{pk} on the surface of the cavity with respect to the acceleration rate E_{acc}. Allowing the peak electric field E_{pk} to increase slightly with respect to E_{acc} was acceptable because the critical magnetic field is a hard limit that cannot be exceeded, whereas the limiting electric field at which field emission starts depends heavily on the surface treatment of the cavity. Previous work used two conjugated elliptical arcs to describe the profile of a reentrant half-cell of a cavity and to minimize the $H_{pk}/\left(42 \cdot E_{acc}\right)$ ratio for $E_{pk}/\left(2 \cdot E_{acc}\right) = 1.2$. These two ratios are used to allow for easier comparison with the TESLA cavity, which has values of one for both $H_{pk}/(42 \cdot E_{acc})$ and $E_{pk}/(2 \cdot E_{acc})$. The optimal shape had an $H_{pk}/\left(42 \cdot E_{acc}\right)$ value of 0.9000. We allowed for more intricately shaped cells by using six conjugated elliptical arcs to construct half-cell profiles, and we tried the optimization for $E_{pk}/\left(2 \cdot E_{acc}\right) = 1.2$ again with this model. Our best result was a reentrant cavity that had $H_{pk}/\left(42 \cdot E_{acc}\right) = 0.8950$, which showed that using six arcs instead of two causes some improvement to the optimization, but the two arc geometry remains a good approach.

I. INTRODUCTION

The development of superconducting radio frequency (SRF) cavities plays a large role in facilitating the progression of accelerators to higher and higher energies. The future International Linear Collider will require approximately 17,000 nine-cell SRF cavities, and

this level of demand calls for more efficient and cost-effective cavities [1]. In recent years SRF cavities have improved dramatically due to better surface preparation techniques that give rise to higher accelerating gradients [2]. These better processing practices can reduce and control the field emission that high electric fields can cause, so electric fields are brought to greater levels within cavities without significant power loss.

These recent improvements in cavity performance through surface preparation techniques have placed more importance on the critical magnetic field, a hard limit that causes the cavity to lose its superconductivity (by "quenching") when reached [3]. Reducing the peak magnetic field H_{pk} within the cavity with respect to the accelerating gradient E_{acc} would allow greater power levels and thus greater accelerating gradients to be reached before the cavity reaches the critical magnetic field. As the peak electric field E_{pk} does not have a hard limit like the peak magnetic field does, we allowed the E_{pk}/E_{acc} ratio to increase in order to decrease H_{pk}/E_{acc}; better surface treatment can be used to control the field emission. Minimizing H_{pk}/E_{acc} at the expense of E_{pk}/E_{acc} by changing the cavity shape has allowed single cell accelerating gradients to reach a record of 52 MV/m for a continuous wave mode on a large niobium cavity [4].

Previous work has found cavity shapes that minimized the H_{pk}/E_{acc} ratio for specific values of E_{pk}/E_{acc} [5–7]. The TESLA cavity provides a convenient point of comparison for these ratios; it has values of $E_{pk}/E_{acc} = 2.0$ and $H_{pk}/E_{acc} = 42$ Oe/(MV/m) [8]. We define e and h as the normalized peak electric and magnetic fields:

$$e = \frac{E_{pk}}{2E_{acc}},\ h = \frac{H_{pk}}{42E_{acc}}, \tag{1}$$

so that e and h are each one for TESLA. Minimizing h for $e = 1.2$ previously produced $h = 0.9000$ using a reentrant cavity half-cell profile described by two conjugated elliptical arcs [5]. We continued work on this $e = 1.2$ case and reduced h to 0.8950 by also using a reentrant cavity but having six conjugated elliptical arcs describe the half-cell profile.

II. SIMULATION AND MODEL

To test out the performance of different cavity shapes we used the SuperLANS code. For a cavity, SuperLANS calculates the maximum electric and magnetic fields inside it, the frequency, accelerating gradient, and the field distributions along the cell profile [9]. This

gave us the means to calculate the e and h values using electric and magnetic field values that have an accuracy on the order of 0.1% for the lowest order mode [10]. The program takes as input the cavity geometry and a mesh of points inside the cavity, and then it performs a numerical analysis on the fields at all of the points to create a holistic picture of the interior fields. Straight lines and elliptical arcs describe the cavity profile, allowing for a lot of freedom in shaping the cell.

Work on minimizing h has shown that reentrant cavities are the best for optimizing h and that nearly identical shapes also minimize the power losses in cavities [11]. Therefore, besides allowing greater accelerating gradients, reentrant shapes can also reduce the cryogenic requirements for SRF cavities. In addition to using a reentrant geometry, shaping the iris of the cavity with an elliptical arc reduces e [11] ; the electric field on the cavity surface is highest along the iris. h is a monotonically decreasing function of e [5, 6], so reducing e by lowering E_{pk} (without increasing h) allows us to reduce h while bringing e back up to its original value. Conversely, we can reduce h at the expense of e initially, and then reduce e back to the original value while maintaining a reduced h. The corresponding approach to reducing h with the cavity shape is to describe the cell's profile with an elliptical arc near the equator [12]. In this manner, the previous work on optimizing h for $e = 1.2$ used two conjugated elliptical arcs to describe a half-cell [5]. The optimized shape has an extended top of the surface magnetic field (H_s) profile curve (see Figure 1); as the magnetic flux is approximately the same between different shapes, this lowers the peak magnetic field [5].

Initially we simulated the shape described by two conjugated elliptical arcs to confirm the merits of the reentrant cavity. Later we described a half-cell profile with six conjugated elliptical arcs so that we could explore more intricately shaped cavities. In a MathCAD program, we input the intersection points and end points of the elliptical arcs, and systems of equations solved for the parameters of the ellipses. The shape was then output to a geometry file that SuperLANS could use. To reduce h for $e = 1.2$, we flattened the electric field profile to lower E_{pk} (since different shapes also have approximately the same electric flux) and also flattened the magnetic field profile to lower H_{pk}.

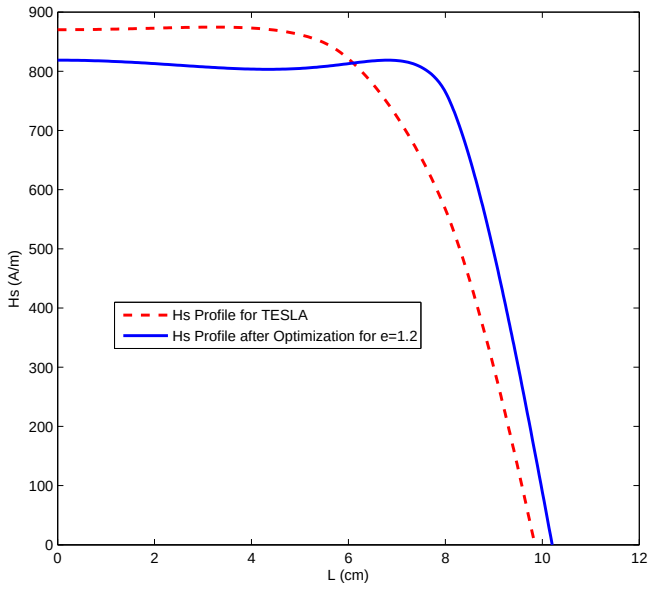

Figure 1: The H_s profiles for the TESLA cavity (dashed red) and the optimized half-cell shape for $e = 1.2$ using two conjugated ellipses (solid blue) [5].

III. REENTRANT CAVITY SIMULATIONS

We first simulated both reentrant and nonreentrant cavity shapes to confirm that the reentrant cavity minimized h more effectively. We used TunedCell, an optimization program that can run SuperLANS for a whole range of input parameters, to perform our simulations. TunedCell describes the half-cell profile with two elliptical arcs that are connected with a straight line segment that is tangent to both arcs [13]. Both a nonreentrant version and a reentrant version of this design are shown in Figure 2. The upper elliptical arc has major and minor half-axes of A and B, respectively, and the lower elliptical arc has a and b as its corresponding half-axes. l denotes the length of the line segment connecting the two arcs.

We allowed A, B, a, and b to vary within certain ranges and let l be solved for by the program. The equatorial radius R_{eq} was adjusted by the program so that all of the cavities had a frequency of 1300 MHz [13]. After starting from a broader range of parameters, we gradually narrowed in on the minimum h for $e = 1.2$ for both the nonreentrant and the reentrant shapes. The parameters for our best solutions are given in Figure 3 below. These results show that the reentrant shape minimizes h more effectively than the nonreentrant one for our case of $e = 1.2$. Therefore, we continued on and simulated more elaborately

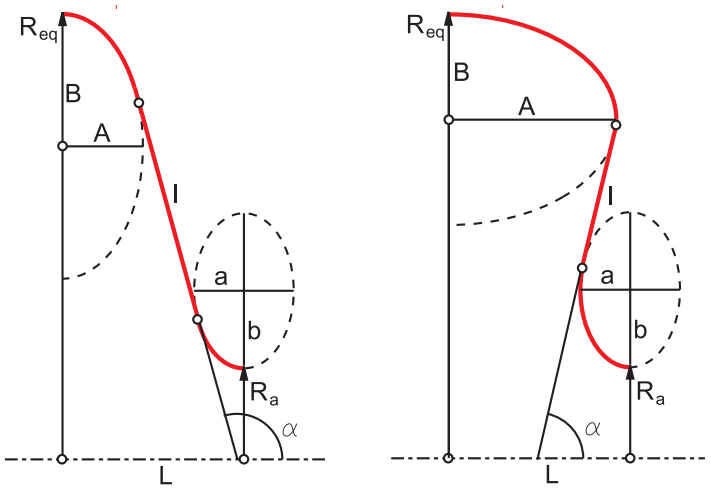

Figure 2: Nonreentrant (left) and reentrant (right) half-cell profiles used by TunedCell.

Figure 3: Table of the parameters for the optimized reentrant and nonreentrant shapes using TunedCell.

Cavity Type	R_{eq} (mm)	A (mm)	B (mm)	a (mm)	b (mm)	l (mm)	e	h
Reentrant	98.711	51.54	36.26	9.18	11.91	0.388	1.1998	0.8995
Nonreentrant	99.421	48.30	33.25	9.35	10.53	20.645	1.1999	0.9167

shaped reentrant cavities to further minimize h.

IV. IMPROVING THE SHAPE

After confirming that the reentrant shape gives the best h values, we allowed for greater variation in shape by describing the half-cell profile with six conjugated elliptical arcs. We tried to change the shape of the cell to flatten the peaks of the electric and magnetic field profiles, both of which would lead to a reduction of h for our $e = 1.2$ case.

A profile using six elliptical arcs is shown in Figure 4, using Z as the major axis and R as the minor axis. We designated the intersection points and the end points between the ellipses as points 0, 1, 2, 3, 4, 5, and 6 moving from the equator to the iris. Points 2 and 4 are defined as the upper and lower points, respectively, where the derivative of the profile is infinity, while point 3 is the inflection point between points 2 and 4.

We can only compare fields between cavities if they are at the same frequency. We "tuned" each cavity to $f = 1300.000 \pm 0.025$ MHz by changing the equatorial radius of each new cell.

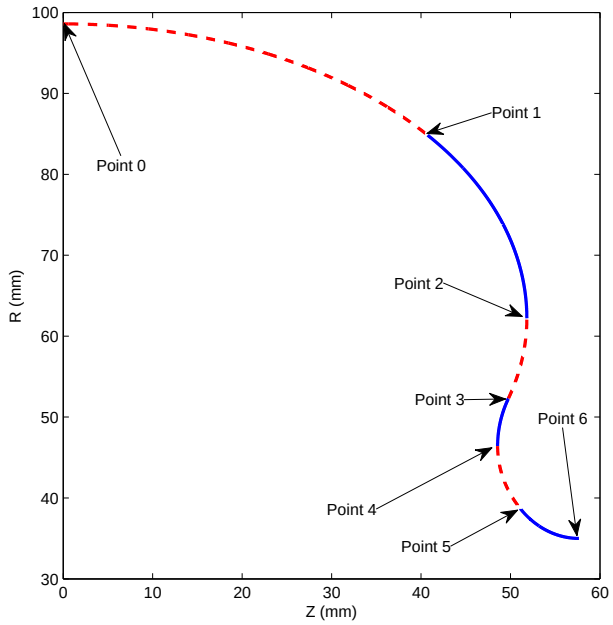

Figure 4: Model of the six conjugated elliptical arcs used to describe a half-cell, alternating between dashed red and solid blue. The intersection points and end points are labeled.

We later adopted a method of proportionally shifting all of the R or Z coordinates above the inflection point (3) to tune the cavities to the given frequency. Our results are valid for any frequency, however, because we can use a proportional change of all dimensions to transition frequencies.

A. Flattening the Electric Field Profile

One important method that we used to reduce h was to flatten the peak of the surface electric field (E_s) profile. This reduced e by lowering E_{pk} and therefore gave us the opportunity to sacrifice e (bringing it back up to 1.2) while reducing h. We could otherwise first sacrifice e to reduce h, and then reduce e by flattening the peak of the electric field profile. The electric field reaches its maximum values near the end of the cell's profile at the iris, and here it peaks just before reaching the end (see Figure 5 "E_s before Transformation"). If we could create a constant electric field over the iris surface, the peak electric field would decrease since the electric flux would remain roughly the same.

We wanted to prevent any increase in h as a result of the flattening because this would

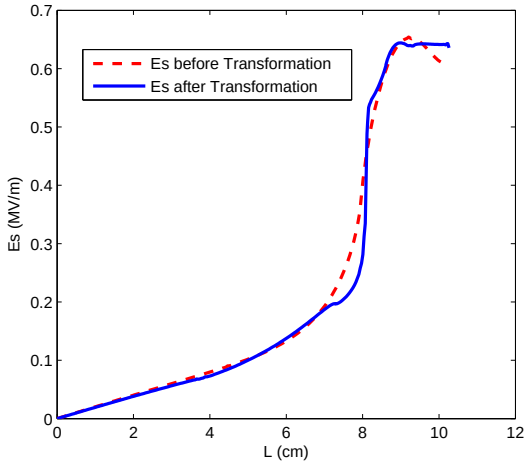

Figure 5: Comparison of the surface electric field profiles before (dashed red) and after (solid blue) the transformation to flatten the peak of the curve.

render the process less effective. A few different changes were able to achieve this. We reduced the curvature of the profile at point 5 and correspondingly increased the curvature at point 4. Flattening the profile near point 5 reduced the E_s values that had previously been the highest, while increasing the curvature at point 4 raised the E_s values there. This evened out the E_s distribution so that E_s was roughly constant along the surface from point 4 to point 6. The transformation also decreased the curvature of the upper elliptical arcs between points 0, 1, and 2 by making the cavity more reentrant, having point 2 pushed to higher Z values. This made the H_s values over the equatorial region more constant so that H_{pk} and thus h were reduced. The two half-cell shapes prior to and after the transformation are given in Figure 6. e dropped by 0.0179 as a result of the flattening, giving us a lot of room to bring h down at the expense of e. Additionally, we not only kept h from increasing, but we also reduced it by 0.0033 as a result of the changes we made in the upper curve.

We now had the means of dropping e by approximately 0.0179 and h by approximately 0.0033. We found the factor that each input parameter changed by during this drop in e, and the set of these factors formed an e-reduction transformation. Then we first reduced h by increasing e; we could apply the e-reduction transformation after this step. Previous work optimized h for e values between 1.0 and 1.5 in increments of 0.1, using two conjugated ellipses to shape the half-cell profile [5]. From the parameters for the $e = 1.2$ and $e = 1.3$

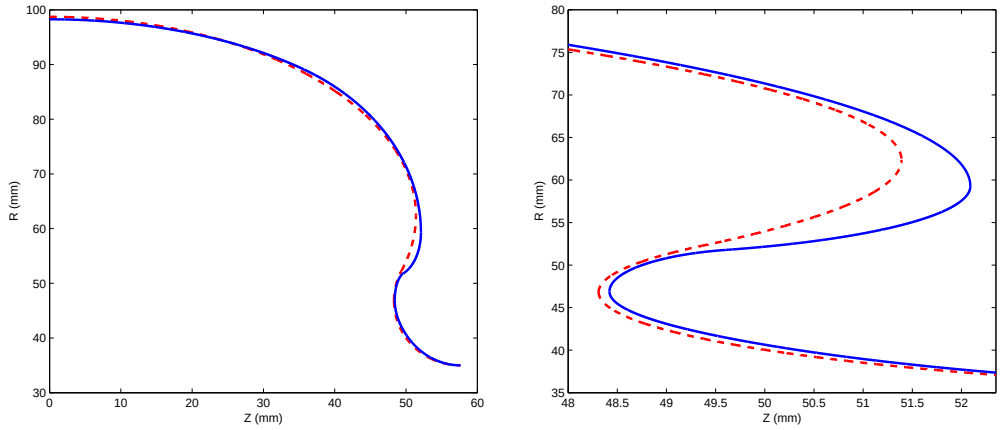

Figure 6: Shape of the right part of the half-cells before (dashed red) and after (solid blue) the transformation to flatten the electric field profile peak. The right display is a closer view of the iris region of the cavities.

cases, we calculated what the parameters would be for an $e = 1.2155$ cavity assuming a linear change in parameters between the two geometries (we found that we could not reduce e by as much as 0.0179 working from e above 1.2). These parameters were used for the six elliptical arcs program (which can reduce to two conjugated ellipses) and this generated a reduced h value of 0.8985. We multiplied our parameters by their respective counterparts in the e-reduction transformation, and this allowed us to reduce e down to 1.1993 while dropping h down to 0.8950.

B. Theoretical Attempt to Flatten the Magnetic Field Profile

Next we attempted to flatten the peak of the magnetic field profile by making the distribution constant near the peak region, thus lowering the peak magnetic field value itself. The equatorial region of the cell has the highest surface magnetic fields. We started out assuming a constant magnetic field H_s on the cavity surface in this region and then derived the shape of the cell profile corresponding with this assumption.

Based on the electric field profile of Figure 5, we approximated the surface electric field in the equatorial region as a linear function of the distance L along the profile from the equator:

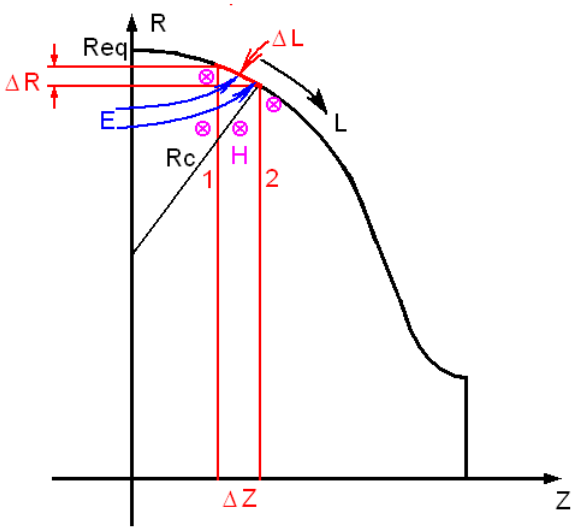

Figure 7: Cavity half-cell profile that depicts sample contours of integration.

$$E_s = \alpha L, \tag{2}$$

in which α is a constant found from a linear least-squares regression of the electric field in the region. Then, using Maxwell's equation $\nabla \times H = \partial D/\partial t$, in which H is the magnetic field and $D = \epsilon E$ is the electric displacement, we wrote an equation relating the electric and magnetic fields inside the cavity:

$$\oint_l H dl = \int_s \frac{\partial D}{\partial t} ds = \int_s \frac{\partial(\varepsilon_0 E)}{\partial t}. \tag{3}$$

Here we integrated along a contour line l that describes surface s; contours are shown in Figure 7, describing cross-sectional surfaces of the cavity perpendicular to the major axis. For contour line 2 of Figure 7, the left hand side of the formula simplifies to $H_s \cdot 2\pi R$. The right hand side is less trivial to solve for, but if we subtract it from the same expression $\int_{s1} \partial(\varepsilon_0 E)/\partial t$ for contour 1, the only electric field in the resulting expression is E_s along the surface region of width ΔL between the two contours. Therefore, subtracting Eq. 3 for contour 2 from the corresponding equation for contour 1, we found that

$$H_s \cdot 2\pi(R + \Delta R) - H_s \cdot 2\pi R = H_s \cdot 2\pi \Delta R = -\omega \varepsilon_0 E_s 2\pi R \Delta L. \tag{4}$$

ω is the angular frequency of the RF power coupled to the cavity. We substituted the expression for E_s from Eq. 2 into the above formula and wrote it as

$$\frac{\Delta R}{R} = \frac{-\omega \varepsilon_0 \alpha L}{H_s} \Delta L. \tag{5}$$

After letting $K = \omega\varepsilon_0\alpha/H_s$, we integrated and solved for R as a function of L:

$$R(L) = R_{eq} \cdot e^{-KL^2/2}. \tag{6}$$

Note that we applied the initial condition that $R(0) = R_{eq}$. Since L is the distance along the profile line, we knew that $(dZ)^2 = (dL)^2 - (dR)^2$ and thus that $dZ = \sqrt{(dL)^2 - (dR)^2} = \sqrt{1 - (dR/dL)^2}dL$. From Eq. 6, we found dR/dL and wrote

$$dZ = \sqrt{1 - R_{eq}^2K^2L^2e^{-KL^2}}dL \Rightarrow Z(L) = \int_0^L \sqrt{1 - R_{eq}^2K^2l^2e^{-Kl^2}}dl. \tag{7}$$

This completes a parametric representation of R and Z as functions of L.

In our MathCAD program that takes the points of a half-cell and fits conjugated elliptical arcs to them, we added several constraints that would help conform the upper elliptical arcs to the theoretical parametric curve. To start out with, we made the radius of curvature of the elliptical arc at point 0 equal that of the parametric curve there. The radius of curvature R_c is given by

$$R_c = \frac{(1 + (\partial R/\partial Z)^2)^{3/2}}{(\partial^2 R/\partial Z^2)}. \tag{8}$$

At the equator, the dependence of R on Z is approximately the same as its L dependence, so we can use $\partial R/\partial L$ and $\partial^2 R/\partial L^2$ in place of $\partial R/\partial Z$ and $\partial^2 R/\partial Z^2$, respectively. Equating the two radii of curvature from the elliptical arc and the parametric curve produces

$$\frac{A_1^2}{B_1} = \frac{1}{K \cdot R_{eq}}, \tag{9}$$

in which A_1 and B_1 are the Z and R half-axes, respectively, of the first elliptical arc. For any K, this equation will force the first elliptical arc to have parameters that have the same radius of curvature as the parametric curve at the equator. We applied a similar technique to match the radius of curvature of the second elliptical arc at point 1 to that of the theoretical curve at the same Z coordinate. The Z dependence of R could not be approximated as the L dependence here, however, so we matched the radii of curvature using Eq. 8 without any approximations. These constraints forced the elliptical arcs to conform closely to the theoretical curve in the equatorial region. The upper elliptical arcs and the theoretical curve are give in Figure 8.

The magnetic field profile corresponding with this shape is given in Figure 9 ("after first iteration"). The peak region does not have a uniform distribution; the field gradually tapers off with increasing L and then experiences a brief rise before falling away.

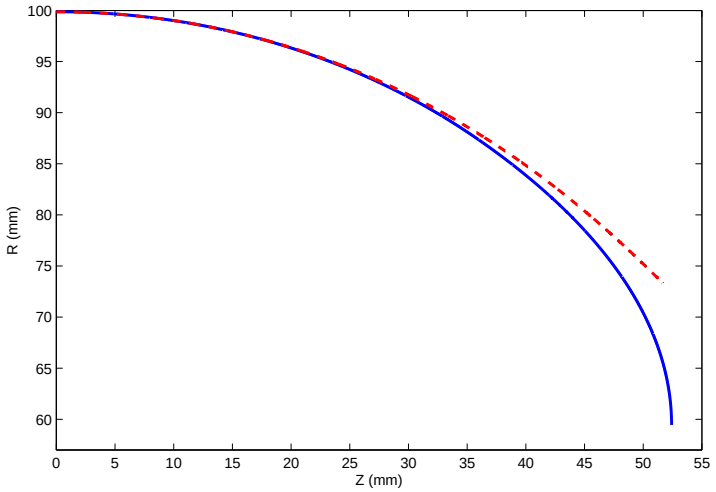

Figure 8: The upper elliptical arc (solid blue) and parametric curve (dashed red) for the first iteration using a linear approximation for E_s.

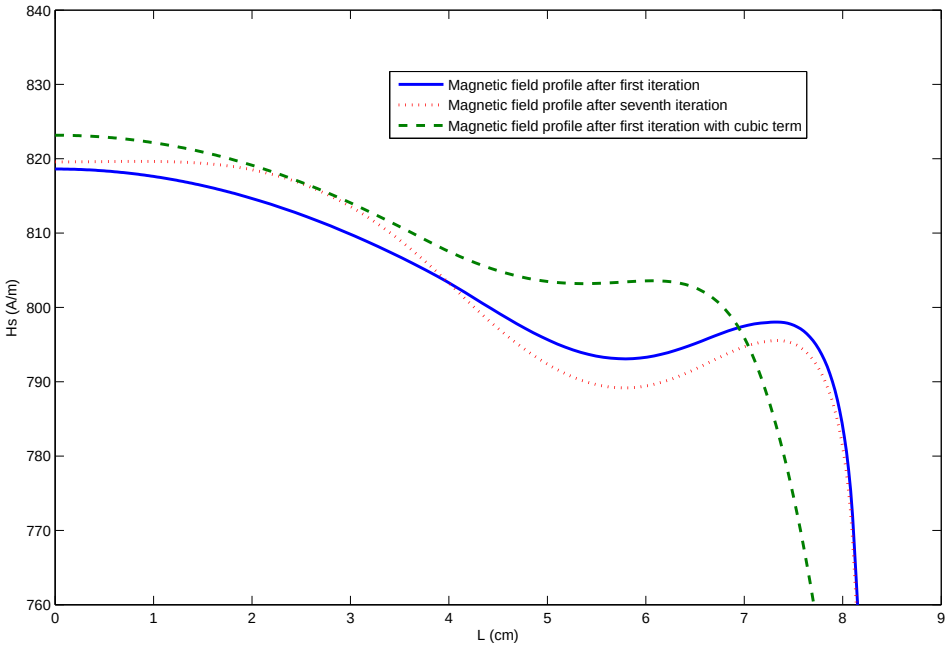

Figure 9: Magnetic field profiles after the first (solid blue) and seventh (dashed red) iterations of the matching process with a linear approximation for E_s. The dashed green line is the magnetic field profile after the first iteration of the matching process with the extra L^3 term included in E_s.

Figure 10: Table of the K, H_{pk}, e, and h values for each of the iterations assuming a linear E_s dependence.

Iteration	Input K ($\times 10^{-4}$ mm^{-2})	Output K ($\times 10^{-4}$ mm^{-2})	H_{pk} (A/m)	e	h
1	1.715	1.985	818.6205	1.1931	0.9032
2	1.985	2.075	818.563	1.1928	0.9033
3	2.075	2.114	819.5454	1.1919	0.9049
4	2.114	2.127	819.605	1.1918	0.9050
5	2.127	2.130	819.6317	1.1918	0.9050
6	2.130	2.132	819.642	1.1918	0.9050
7	2.132	2.132	819.645	1.1918	0.9050

The electric field profile for this shape would ideally have the same linear dependence in the equatorial region as the profile that we found our K value with, for the new geometry was based off of this value of K. However, this was not initially the case, so we refit the new profile and found a new K. We adopted this K value in the program and created a new shape. We proceeded iteratively in this manner, finding a new K, making the shape, and checking the K, until the input K into the model was the same as the output K. The iterations' K values are given in Table 1. The magnetic field profiles of the shapes from the first and the last iterations were similar (see Figure 9), but neither one produced a flat peak. Using a linear approximation for the electric field in the equatorial region was not sufficient to flatten the magnetic field profile.

The electric field profile itself has a slight curvature in the equatorial region that is consistent with an odd function of L. To better describe the profile, we incorporated an L^3 term into our description of E_s so that

$$E_s = \alpha L + \beta L^3. \tag{10}$$

This could potentially bring about the improvement in the magnetic field profile that we desired. Going through the same process as Eqs. 5 through 7 with this new form of E_s and then letting $K = \omega\varepsilon_0\alpha/H_s$ and $M = \omega\varepsilon_0\beta/H_s$ produced

$$R(L) = R_{eq} \cdot e^{-\left(KL^2/2 + ML^4/4\right)} \tag{11}$$

and

$$Z(L) = \int_0^L \sqrt{1 - Req^2 \cdot (Kl + Ml^3)^2 e^{-(Kl^2 + Ml^4/2)}} dl. \tag{12}$$

We used these forms to modify our equations of constraint in our MathCAD program. We matched the curvature of the theoretical curve with the first elliptical arc at point 0 and with the second elliptical arc at point 1 using equations 9 and 8 respectively. To match the curve further along the elliptical arcs, we defined point 2 as the point at which the theoretical curve has $\partial R/\partial L = -1$ (here we call $L = L_{max}$) so that

$$\frac{\partial R}{\partial L} = -1 = -R_{eq} \cdot e^{KL_{max} + ML_{max}^3}. \tag{13}$$

With fixed K and M values, we solved for L_{max}, $R(L_{max})$, and $Z(L_{max})$ and set the latter two as the coordinates of point 2. This ensured that the elliptical arc coincided with the theoretical curve there. At very low L, the L^3 term is negligible, so we solved for α (and then K) the same way as we did the previous case: fitting the electric field profile to a line for the lowest L values . We then plotted $\log(E_s - \alpha L)$ vs. $\log L$ for the equatorial region extending to approximately point 2 , since

$$\log(E_s - \alpha L) = \log(\beta L^3) = \log \beta + 3 \cdot \log L, \tag{14}$$

and fit the data to a line. The constant term in the regression line equation is $\log \beta$, so we solved for β (and then M) in this manner.

We worked through the same iterative process with this new dependence that we did with the linear case. We found K and M for a shape, put these values back into our MathCAD program to generate a new geometry, and checked K and M. The magnetic field profile after one iteration is given in Figure 9. The profile has higher magnetic field values in the equatorial region than the other profiles derived from the linear approximation, and also the peak region is shorter, falling off before the others. The electric field profile of the first iteration gives rise to a β (and M) value several orders of magnitude below the original value. The MathCAD program cannot find a solution using this M, since the theoretical curve does not have a point at which $\partial R/\partial L = -1$, so we only could go through one step of the iteration process.

Basing our upper arcs on a theoretical curve from a linear approximation of E_s, and then also with an incorporated L^3 term, did not flatten our magnetic field profile. We therefore did not lower h from our previous value.

V. DISCUSSION AND CONCLUSION

We first used TunedCell to verify that the reentrant cavity profile is the most effective geometry for minimizing h. From here we worked with a more complicated six elliptical arcs model of reentrant cavities and tried several different ways to further minimize h for $e = 1.2$. Flattening the peak of the electric field profile reduced e without sacrificing h, and this let us start with a reduced h and elevated e and then reduce e back to 1.2. This gave us our best value of h at 0.8950. While flat, the peak of the electric field profile still represents a small fraction of the cavity's profile. Extending the peak over a larger region would lower the peak values and reduce e even more. The electric field would need to be raised in the region of the profile between points 3 and 4, and making the elliptical arc have greater curvature here could accomplish this goal. This possibility should be explored in the future.

Our attempt to produce a constant magnetic field in the equatorial region of the cavity by basing the upper arcs on a theoretically derived curve did not succeed. The peak region of the cavity's magnetic field profile still was not uniform. We worked from Maxwell's equation and first used the assumption that E_s was linear in the equatorial region before incorporating a L^3 term into the dependence. Perhaps we need a more sophisticated description of the E_s dependence in order to flatten the magnetic field peak, or perhaps we could incorporate other constraints into our MathCAD program to better fit our elliptical arcs to the theoretical curve.

Our six conjugated elliptical arcs used to describe a cavity's half-cell profile allowed us to improve the minimization of h for $e = 1.2$ to $h = 0.8950$. The two conjugated elliptical arcs that were previously used ($h = 0.9000$ from optimization) are a simplified yet still effective way of optimizing the shape.

VI. ACKNOWLEDGMENTS

I would like to thank my mentor Valery Shemelin of Cornell University for guiding me through this research project and for teaching me a great deal about SRF cavities and accelerator physics. I also would like to acknowledge Rich Galik, Ernie Fontes, Monica Wesley, and Lora Hines for running the Research Experience for Undergraduates program

at CLASSE and for making the summer a great experience. Ed Lochocki and Fangfei Shen provided valuable assistance for my work in MatLab. This work was supported by the National Science Foundation REU grant PHY-0849885.

VII. REFERENCES

[1] James Brau, James Okada, and Nicholas Walker. International Linear Collider Reference Design Report: ILC Global Design Effort and World Wide Study. August 2007.

[2] H. Padamsee. *RF Superconductivity:Science, Technology, and Applications.* WILEY-VCH Verlag GmbH & Co., 2009.

[3] K. Saito. Theoretical Critical Field in RF Application. *KEK, Accelerator Lab, 1-1*, 2003.

[4] R.L. Geng. Review of New Shapes for Higher Gradients. *Physica C Superconductivity*, 441:145–150, July 2006.

[5] V. Shemelin, H. Padamsee, and R. L. Geng. Optimal cells for TESLA accelerating structure. *Nuclear Instruments and Methods in Physics Research A*, **496**:1–7, January 2003.

[6] V. Shemelin and H. Padamsee. The Optimal Shape of Cells of a Superconducting Accelerating Section. *Cornell University LNS Report, SRF 020128-01/TESLA Report 2002-01*, 2002.

[7] V. Shemelin, R. Geng, J. Kirchgessner, H. Padamsee, and J. Sears. An Optimized Shape Cavity for TESLA: Concept and Fabrication. In *Proceedings of the 2003 IEEE Particle Accelerator Conference (PAC 03). 12-16 May 2003, Portland, Oregon. 20th IEEE Particle Accelerator Conference, p.1314*, 2003.

[8] B. Aune, R. Bandelmann, D. Bloess, B. Bonin, A. Bosotti, M. Champion, C. Crawford, G. Deppe, B. Dwersteg, D. A. Edwards, H. T. Edwards, M. Ferrario, M. Fouaidy, P.-D. Gall, A. Gamp, A. Gössel, J. Graber, D. Hubert, M. Hüning, M. Juillard, T. Junquera, H. Kaiser, G. Kreps, M. Kuchnir, R. Lange, M. Leenen, and M. Liepe. Superconducting TESLA cavities. *Phys. Rev. ST Accel. Beams*, 3(9):092001, Sep 2000.

[9] D. Myakishev, V. Yakovlev, M. Tiunov, and O. Danilov. SUPERLANS/SUPERSAM Codes: User's Guide. December 1992.

[10] S. Belomestnykh. Spherical cavity: Analytical formulas. comparison of computer codes. In

Cornell University LNS report SRF 941208-13, 1994.

[11] V. Shemelin. Reentrant Cavities have Highest Gradient and Minimal Losses Simultaneously. *Cornell University LEPP Report, SRF051010-09*, 2005.

[12] V. D. Shemelin. Low Loss and High Gradient SC Cavities with Different Wall Slope Angles. In *Proceedings of the 2007 IEEE Particle Accelerator Conference (PAC 07). 25-29 Jun 2007, Albuquerque, New Mexico. 22nd IEEE Particle Accelerator Conference, p.2352*, 2007.

[13] Dmitry Myakishev. TunedCell. *Cornell University LEPP Report, SRF/D 051007-02.*